Received: 2 April 2020 | Accepted: 25 June 2020

DOI: 10.1002/hyp.13857

RESEARCH ARTICLE

WILEY

Near-real-time one-kilometre Soil Moisture Active Passive soil moisture data product

Jifu Yin[1,2] | Xiwu Zhan[2] | Jicheng Liu[3] | Hamid Moradkhani[4] | Li Fang[1,2] | Jeffrey P. Walker[5]

[1]ESSIC/CISESS, University of Maryland College Park, College Park, Maryland

[2]NOAA NESDIS Center for Satellite Applications and Research, College Park, Maryland

[3]Laboratory of Environmental Model & Data Optima, Laurel, Maryland

[4]Center for Complex Hydrosystems Research, Department of Civil, Construction and Environmental Engineering, University of Alabama, Tuscaloosa, Alabama

[5]Department of Civil Engineering, Monash University, Clayton, Australia

Correspondence
Jifu Yin, Earth System Science Interdisciplinary Center (ESSIC), University of Maryland, 5825 University Research Court Suite 4001, College Park, MD 20740.
Email: jyin@umd.edu

Funding information
NASA SMAP Science Utilization Program; NOAA JPSS Proving Ground and Risk Reduction (PGRR) Program; NOAA's Climate Program Office's Modeling, Analysis, Predictions

Abstract

The coarse resolution soil moisture (SM) data from NASA SMAP mission have been steadily produced with the expected performance since April 2015. These coarse resolution observations could be downscaled to fine resolution using fine scale observations of SM sensitive quantities from existing satellite sensors. For operational users who need near-real-time (NRT) high resolution SM data, the downscaling approach should be feasible for operational implementation, requiring limited ancillary information and primarily depending on readily available satellite observations. Based on these principles, nine potential candidate downscaling schemes were selected for developing an optimal downscaling strategy. Using remotely sensed land surface temperature (LST) and enhanced vegetation index (EVI) observations, the optimal downscaling approach was tested for operational producing a NRT 1 km SM data product from SMAP. Comprehensive assessments on the 1 km SM product were conducted based on agreement statistics with in-situ SM measurements. Statistical results show that the accuracy of the original coarse spatial resolution SMAP SM product can be significantly improved by 8% by the downscaled 1 km SM. With respect to the in-situ measurements, the 1 km SM mapping capability developed here presents a clear advantage over the SMAP/Sentinel SM data product; and it also provides better data availability for users. This study suggests that a NRT 1 km SMAP SM data product could be routinely generated from SMAP at the centre for Satellite Applications and Research of NOAA NESDIS for operational users.

KEYWORDS

downscale, near real time, SMAP, soil moisture, spatial resolution

1 | INTRODUCTION

Soil moisture (SM) plays a critical role in exchange of water, energy and carbon between the land surface and the atmosphere (Yin et al., 2014). It controls the SM-precipitation feedback at continental scale and runoff-precipitation response at watershed scale. As a result, SM observations are widely used in meteorology, hydrology and climatology (Peng, Loew, Merlin, & Verhoest, 2017; Yin, Hain, Zhan, Dong, & Ek, 2019; Yin, Zhan, Hain, Liu, & Anderson, 2018). The development of ground-based SM measurement techniques provides an opportunity to obtain SM estimates at different soil depths (Robinson et al., 2008, Dobriyal et al., 2012, Vereecken et al., 2014) with the in situ observations commonly considered as the "truth" to validate satellite and model SM simulations against. However, such ground measurements typically have sparse spatial distributions which cannot represent SM patterns at even regional let alone global scale.

Microwave remote sensing has shown a unique capability for quantitative estimating of SM dynamics at regional and global scales

(Jackson & O'Neill, 1990; Jackson & Schmugge, 1989; Wang, ET Engman, Mo, & Schmugge, 1987). C- and X-band SM data products have been operationally produced since 2001, which include the Advanced Scatterometer (Wagner et al., 2013), Advanced Microwave Scanning Radiometer for Earth Observing System (AMSR-E) (Njoku, Jackson, Lakshmi, Chan, & Nghiem, 2003), AMSR2 (JAXA, 2013) and WindSat (Li et al., 2010). However, they suffer from the relatively short observation wavelength. Because L-band microwave remote sensing is sensitive to a deeper subsurface SM (0–5 cm) and relatively insensitive to vegetation (Colliander et al., 2017), the Soil Moisture and Ocean Salinity (SMOS) and Soil Moisture Active Passive (SMAP) satellites have been developed (Entekhabi et al., 2010; Kerr et al., 2010). Compared to SMOS, SMAP presents a more accurate SM retrieval due to it can reduce impact by Radio Frequency Interference (RFI) contamination and its better antenna design (Chan et al., 2016). Passive L-band microwave remote sensing has also been generally accepted to have reduced impacts from surface roughness and the atmosphere (Kerr, 2007). Despite the observed brightness temperature (Tb) having a more direct connection with the surface SM in the L-band frequency regime, they suffer from having a moderately coarse spatial resolution (Piles et al., 2011; Wu, Walker, Rüdiger, Panciera, & Gao, 2017), due to field of view being inversely proportion to the wavelength.

Radars, especially synthetic aperture radars (SARs), can provide higher spatial resolution SM, although the sensitivity of active microwave observations is more subject to surface roughness impact. However, it had been shown by several studies that there is a potential to enhance the spatial resolution of the retrieved SM by merging the coarse but accurate precision microwave retrieval with the noisy but fine resolution radar observations. SMAP was thus launched in 2015 to address the scale issue by using 3 km resolution active microwave measurements to downscale the 40 km resolution passive microwave SM retrievals (Entekhabi et al., 2010). In preparation for the SMAP mission, many approaches were proposed to explore the feasibility of merging radar backscatter and radiometer Tb observations, such as the Bayesian merging method (Zhan, Houser, Walker, & Crow, 2006), Triangular method (Merlin, Chehbouni, Kerr, & Goodrich, 2006), Change Detection of Radar Backscatter (Narayan, Lakshmi, & Jackson, 2006), Deterministic Method (Merlin et al., 2008), and the Combined Modelling and Remote Sensing method (Merlin, Chehbouni, Kerr, Njoku, & Entekhabi, 2005). However, the reported results only provide testable explanation and their representativeness at the global and multiyear scales was not addressed (Sabaghy, Walker, Renzillo, & Jackson, 2018; Zhan et al., 2006). After SMAP was launched, the baseline and optional downscaling algorithms were officially implemented to produce fine resolution SM retrievals along with assuming a near linear relationship between radar backscatter and radiometer Tb data (Das et al., 2014; Entekhabi et al., 2014; Wu et al., 2017). With the loss of SMAP's L-band radar from July 7, 2015, the capability of SMAP's providing a 3 and 9 km resolution SM product was lost (Yin & Zhan, 2018).

Optical and thermal infrared satellite SM sensing started in the 1970 with several approaches developed to exploit the relationships between surface reflectance and SM (Carlson, Gillies, & Perry, 1994; Liu et al., 2002). When SM is low, evaporative cooling may be low and in turn results in higher land surface temperature (LST). A wetter land surface generally helps plant growth and thus a higher vegetation index value observed from optical/infrared satellite sensors. Unlike microwave remote sensing, optical and thermal satellite sensors provide finer spatial resolution (Peng et al., 2017). To overcome the coarse spatial scale limitation of the relatively accurate microwave radiometer SM data, recent attempts to generate higher spatial resolution L-band measurements using the fine scale vegetation index and LST observations have been well documented (Table 1). However, the addition of surface albedo does little to enhance downscaled SM estimates (Knipper et al., 2017; Wu et al., 2017). Specifically, empirical polynomial fitting or regression methods typically exploit the relationships between L-band SM and optical/thermal observations (Table 1). Given correlations between SM and geoformation data, topography is also generally used as ancillary information within the downscaling approaches (Peng et al., 2017). Long-term dense in situ SM observations allow training regression models to generate finer resolution SM retrievals; however, operational application of these empirical polynomial fitting methods is hampered by requirements of extensive in situ SM observations (Abbaszadeh et al., 2019; Senanayake et al., 2019; Zhao et al., 2018). Optimizing land surface model (LSM) variables to provide fine-scale SM estimations for the overlapping coarse resolution pixels is also proposed to downscale L-band SM observations; yet differences in climatology between remote sensing and LSM SM estimates limit their applicability (Fang et al., 2018). The semi-physical evaporation-based methods (Colliander et al., 2017; Mishra et al., 2018) are possible to obtain disaggregated SM at finer resolution and have been proposed to operationally generate a SMOS disaggregated SM product (Molero et al., 2016). Yet, the reasonable performance of the evaporation-based fine scale SM in semi-arid regions cannot mirror the good behaviour in wet areas. Based on the Neural-network approach, using the monthly Normalized difference vegetation index (NDVI) and topographic index, a 2.25 km SMAP SM data product is reported, but it is unable to retrieve fine resolution SM near coastal regions or for high vegetation covered areas (Alemohammad et al., 2018). After the SMAP L-band radar stopped operation, integration of L-band radiometer brightness temperature (Tb) and C-band Sentinel-1A SAR backscatter observations was recognized as a feasible approach to produce fine scale SMAP SM data (Das et al., 2019; He et al., 2018; Li et al., 2018). However, few studies have conducted inter-comparisons of performances at large scale between C-band SAR- and optical/thermal observations-based downscaling fine resolution SM data. Table 1 also shows that ideally results with low uncertainties were generally documented in semi-arid areas, but the feasibility of implementing them for operational product generation is still unknown.

Current operational satellite SM data products are at a spatial resolution as coarse as 40 km (Yin et al., 2015; Yin, Zhan, Liu, & Schull, 2019) at National Oceanic and Atmospheric Administration (NOAA). However, operational applications such as numerical weather and seasonal climate predictions, agricultural drought and flood

TABLE 1 Summary of the commonly used L-band downscaling methods during the 2015–2019 period

Method	Ancillary info	Study region	Climate	Study period	Accuracy	Reference
Simplified water-cloud model	Sentinel-1A SAR backscatter	Southern Ontario, Canada	Semiarid	May and July of 2016	ubRMSE = 0.05 m^3/m^3	Li, Wang, Gunn, Joosse, & Russell, 2018
Regression tree model	LST, long-term in situ SM, NDVI, land cover and soil texture	Goulburn River catchment, Australia	Semiarid	2015–2016	Enhanced 9 km: ubRMSE = 0.07 m^3/m^3 Enhanced 25 km: ubRMSE = 0.05 m^3/m^3	Senanayake et al., 2019
Ensemble learning method	NDVI, LST, precipitation, elevation, soil texture, and in situ SM	CONUS	—	April 1, 2015 ~ December 31, 2015	ubRMSE = 0.047 m^3/m^3 for SCAN, ubRMSE = 0.040 m^3/m^3 for USCRN,	Abbaszadeh, Moradkhani, & Zhan, 2019
Random Forest regression	LST, LAI, NDVI, EVI, albedo, NDWI, elevation, slope, and aspect	Iberian Peninsula	Semiarid	April 12,015 to December 31, 2016	ubRMSE = 0.022 m^3/m^3	Zhao, N Sánchez, & Li, 2018
Thermal inertia theory	NDVI, model surface skin Temperature and 0–10 cm SM, LST	WGEW, Arizona, USA	Semiarid	August 2015	ubRMSE = 0.009 ~ 0.02 m3/m3	Fang, Lakshmi, Bindlish, & Jackson, 2018
Neural-network	Monthly NDVI, topographic index	Global	—	April 1, 2015 until march 31, 2017	ubRMSE = 0.065 m3/m3	Alemohammad, Kolassa, Prigent, Aires, & Gentine, 2018
Second-order polynomial regression formula	Night LST, and EVI	WGEW, Arizona, USA	Semiarid	April 1, 2015 ~ October 4, 2016	ubRMSE = 0.42 ~ 0.046 m^3/m^3 for SMOS and ubRMSE = 0.036 ~ 0.037 m^3/m^3 for SMAP	Knipper, Hogue, Franz, & Scott, 2017
Soil evaporative efficiency-soil moisture relationship	NDVI, LST	Southern Arizona, USA	Semiarid	August 2015	ubRMSE = 0.035 m^3/m^3	Colliander et al., 2017
DISPATCH	Model temperature, elevation, ALEXI evaporation	CONUS	—	Apr 2015–Nov 2016	0.062 to 0.064 m^3/m^3	Mishra et al., 2018

Abbreviations: LST, NDVI, EVI and NDWI indicate land surface temperature, normalized difference vegetation index, enhanced vegetation index and normalized difference water index, respectively. Abbreviations DISPATCH, ALEXI and WGEW are DISaggregation based on Physical And Theoretical scale CHange, Atmospheric Land EXchange Inverse and Walnut Gulch Experimental Watershed, respectively.

monitoring and wildfire risk assessment, require near real time (NRT) finer resolution SM data. This study therefore proposes an operationally feasible approach to providing a high resolution SMAP SM data product at the centre for SaTellite Applications and Research (STAR) of NOAA. Three downscaling algorithms were selected in this paper due to their significance and representativeness and inter-compared including evaluation against the SMAP/Sentinel 3 km product. An operational pathway of the 1 km soil moisture product is also described.

2 | DATASETS

2.1 | SMAP 25 km SM

The SMAP satellite was launched on January 31, 2015 to an altitude of around 685 km and began to provide science data on April 1, 2015. It was designed to provide the 2–3 day fine resolution SM required for hydrology, climatology and meteorology by merging L-band radar and radiometer data (Entekhabi et al., 2010). The SMAP mission was targeted to measure top 5 cm surface SM with retrieval errors below 0.04 m^3/m^3, with the L-band radar and L-band radiometer sensors on SMAP designed to penetrate vegetation with vegetation water content up to 5 kg/m^2 (Entekhabi et al., 2010). With loss of the L-band radar on July 7, 2015, however, the SMAP satellite lost its capability to directly provide high resolution global soil moisture data products. Fortunately, the SMAP L-band radiometer has been successfully and continuously providing high quality coarse resolution Tb observations (Yin, Zhan, et al., 2019) enabling the operational production of level-2 SM data products (Colliander et al., 2017; Reichle et al., 2017). The L-Band radiometer on the SMAP satellite offers 40 km resolution Tb observation with ±1.3 K radiometric uncertainty. Note that SMAP SM observations were resampled to a regular 25 km × 25 km grid in this paper. The SMAP v5.0 (SMAPV5) SM data used here were obtained from National Snow and Ice Data Center.

2.2 | SMAP/sentinel 3 km SM product

After loss of the SMAP L-band radar, merging C-band radar and L-band radiometer data was proposed to recover the capability of producing fine resolution SM (Das et al., 2016). The orbit configuration of Sentinel-1A is similar to that of SMAP, meaning that their swaths overlap with minimal time difference. Consequently, it has been recognized that the C-band SAR data from Sentinel-1A observations can be used as a substitute for the SMAP radar (Das et al., 2019). Specifically, the SMAP/Sentinel (SPL2SMAP) product combines the coarse resolution SMAP Tb with the 3 km C-band backscatter measurements from the Sentinel-1A SARs to provide 3 km SM data (Das et al., 2019). It is important to note that the C-band radar on Sentinel-1 is not a perfect replacement for SMAP's lost L-band radar, but it is the only radar trailing SMAP closely enough to improve the SMAP's radiometer measurements. The SPL2SMAP SM data from NASA (National Aeronautics and Space Administration) Jet Propulsion Laboratory (JPL) are used to conduct complementary evaluations on the optimal downscaling strategic.

2.3 | VIIRS LST data product

The Visible Infrared Imaging Radiometer Suite (VIIRS) instrument is a primary sensor onboard the S-NPP satellite that was launched on October 28, 2011. It is designed to provide operational observation continuity with the Advanced Very High Resolution Radiometer (AVHRR) and MODerate resolution Imaging Spectroradiometer (MODIS). VIIRS provides 750-m LST observations at nadir during the S-NPP satellite overpass time at 1:30 am/pm local time (Liu, Yu, Yu, Göttsche, & Trigo, 2015). The VIIRS level 2 LST data product began from January 19, 2012. The validation results demonstrated that the VIIRS LST has a good agreement with ground LST measurements (Liu et al., 2015; Liu, Yu, Yu, Wang, & Rao, 2019). The level 3 daily gridded VIIRS LST data with 1 km spatial resolution has been locally generated at NOAA-STAR since May 3, 2017. The operational level 3 VIIRS LST will be operational in the near future. As the three selected downscaling approaches require the LST, the 1 km VIIRS LST data were used in this paper.

2.4 | Enhanced vegetation index

Compared to the NDVI, the enhanced vegetation index (EVI) was developed to reduce the aerosol contaminations and canopy background brightness variations (Huete et al., 2002). Both the MYD13A2 V6 product from Aqua observations and MOD13A2 V6 product from Terra measurements provide 16-day composites of the 1 km EVI retrievals, which permit an eight-day phasing in the EVI production through combining both data records. The EVI uses a MODIS-specific compositing method that removes low quality pixels on the basis of product quality assurance metrics. In this study, the gridded 8-day 1 km MODIS EVI data are those distributed by NASA. Compared to the 90-day achieving period of VIIRS EVI in the NOAA, MODIS provides continuous and reliable long-term EVI data, which allow the statistical results in this paper to represent a longer analysis period. Note that cross-sensor compatibilities of the EVI data between VIIRS and MODIS indicate that their systematic differences are less than 2% (Miura, Muratsuchi, & Vargas, 2018). It should thus be expected to obtain similar results are obtained using VIIRS EVI as ancillary information in future operation. The 1 km EVI data were employed here to satisfy the requirements of the three selected downscaling methods.

2.5 | SCAN in situ observations

The US Department of Agriculture Soil Climate Analysis Network (SCAN) provides hourly measurements with automatic devices measuring the soil dielectric constant at depths of 5, 10, 20, 50 and

100 cm where soil depth permits (Schaefer et al., 2007). The data sets from each SCAN site were quality controlled by detecting problematic observations. Specifically, SM measurements outside of the physically possible range were excluded (Liu et al., 2011). The SM observations under frozen conditions were also excluded on basis of SCAN soil temperature measurements for the corresponding soil layer (Yin et al., 2016; Yin, Zhan, et al., 2015). The quality controlled 5 cm SCAN SM observations were then aggregated into daily averages. Station SM records with data coverage below 70% (510 days) over the May 3, 2017–April 30, 2019 period were also excluded (Yin et al., 2015). Finally, the SM observations from the 148 stations were used in this study.

3 | METHODOLOGY

With the aim to operationally generate a NRT fine resolution SMAP SM data product at the NOAA-STAR, the downscaling method should include pure dependent on satellite measurements, have limited ancillary information requirements, be computationally fast, and feasible to implement as an automated routine. Based on the fine scale observations from the Suomi National Polar-orbiting Partnership (S-NPP), three classical optical/thermal and microwave fusion approaches were inter-compared, including (a) the triangular method (Carlson et al., 1994; Petropoulos, Carlson, Wooster, & Islam, 2009), (b) the vegetation temperature condition index (VTCI) method (Peng, Loew, Zhang, Wang, & Niesel, 2016; Wan, Wang, & Li, 2004), and (c) soil wetness index (SWI)-based UCLA method (Jiang & Islam, 2003; Kim & Hogue, 2012). Utilizing EVI and different LST information, including daytime, nighttime and day-time LST difference (DTR), nine downscaling schemes were designed and tested to find out the optimal downscaling strategy.

3.1 | Triangle method

The temperature–vegetation TRIAngle (TRIA) treats limited water availability at the "dry edge" and unlimited water access at the "wet edge" (Sandholt et al., 2002). The LST is sensitive to SM over bare soil areas, whereas the vegetation index has high sensitivity to SM over vegetated regions (Carlson et al., 1994; Peng et al., 2017). As a result, SM is parameterized based on a triangular distribution of fine resolution LST and EVI. The regression relations can be expressed as

$$\mathrm{SMAP} = \alpha \overline{\mathrm{EVI}^* X^*} + \beta \tag{1}$$

where SMAP is the gridded 25 km SMAP SM. Variables α and β are the slope and intercept, respectively. While $\overline{\mathrm{EVI}^*}$ and $\overline{X^*}$ are given by

$$\overline{\mathrm{EVI}^*} = \frac{1}{mn}\sum_{i=1}^{i=n}\sum_{j=1}^{j=m}\mathrm{EVI}^* \tag{2}$$

$$\overline{X^*} = \frac{1}{mn}\sum_{i=1}^{i=n}\sum_{j=1}^{j=m}X^* \tag{3}$$

where both m and n are 25 in this paper and EVI^* and X^* are defined as (Kim & Hogue, 2012)

$$\mathrm{EVI}^* = \frac{\mathrm{EVI} - \mathrm{EVI}_{\min}}{\mathrm{EVI}_{\max} - \mathrm{EVI}_{\min}} \tag{4}$$

$$X^* = \frac{X - X_{\min}}{X_{\max} - X_{\min}} \tag{5}$$

The subscripts max and min indicate the maximum and minimum EVI or X over the study area, respectively. Based on the established relationship, the 1 km SM (DSM) can be calculated by

$$\mathrm{DSM} = \alpha \mathrm{EVI} \times X + \beta \tag{6}$$

where the downscaling schemes are recognized as TRIA_DAY, TRIA_NIGHT and TRIA_DTR when the variable X represents day-time LST, night-time LST and DTR, respectively.

3.2 | VTCI method

According to the temperature–vegetation Triangle, the increasing LST is reflected at the "dry edge" due to low SM limits on evapotranspiration which in turn to raise LST, whereas unlimited SM and maximum evapotranspiration are formed at the "wet edge" (Sandholt et al., 2002). The VTCI is thus calculated for each EVI interval (Peng et al., 2017)

$$\mathrm{VTCI} = \frac{X_{\max} - X}{X_{\max} - X_{\min}} \tag{7}$$

where the subscripts max and min indicate the maximum and minimum X that have the same EVI value. Particularly, the VTCI_DAY, VTCI_NIGHT and VTCI_DTR are downscaling schemes with the corresponding X representing day-time LST, night-time LST and DTR, respectively. The relationship between 1 km SM (DSM) and VTCI is given by

$$\mathrm{DSM} = \mathrm{VTCI} \times \frac{\mathrm{SMAP}}{\frac{1}{mn}\sum_{i=1}^{i=n}\sum_{j=1}^{j=m}\mathrm{VTCI}} \tag{8}$$

3.3 | UCLA method

Based on the triangle interpretation of vegetation index and LST, Jiang and Islam (2003) proposed a simple method to retrieve evaporative fraction, which can also be used as a soil wetness index (SWI) defined as (Kim & Hogue, 2012)

$$SWI = 1 - \frac{(1-\varphi EVI)\Delta X}{(1-EVI)\Delta X_{max} + EVI\Delta X_e} \quad (9)$$

where X_e indicates the maximum X when the EVI value is roughly 1.0, and ΔX, ΔX_{max}, ΔX_e and φ are expressed as

$$\Delta X = X - X_{min} \quad (10)$$

$$\Delta X_{max} = X_{max} - X_{min} \quad (11)$$

$$\Delta X_e = X_e - X_{min} \quad (12)$$

$$\varphi = 1 - \frac{\Delta X_e}{\Delta X_{max}} \quad (13)$$

The downscaling schemes are recognized as UCLA_DAY, UCLA_NIGHT and UCLA_DTR when the X represents day-time LST, night-time LST and DTR, respectively. The 1 km SMAP SM is then derived by

$$DSM = SWI \times \frac{SMAP}{\frac{1}{mn}\sum_{i=1}^{i=n}\sum_{j=1}^{j=m} SWI} \quad (14)$$

3.4 | Performance measures

Based on the quality controlled SCAN SM observations (O), evaluation metrics in this paper include correlation coefficient (r), root mean square error (RMSE) and unbiased RMSE (ubRMSE), which can be expressed as

$$r_{M,O} = \frac{\sum_{i=1}^{i=n}(M_i-\bar{M})(O_i-\bar{O})}{\sqrt{\sum_{i=1}^{i=n}(M_i-\bar{M})^2\sum_{i=1}^{i=n}(O_i-\bar{O})^2}} \quad (15)$$

$$RMSE = \sqrt{\frac{\sum_{i=1}^{i=n}(M_i-O_i)^2}{n}} \quad (16)$$

$$ubRMSE = \sqrt{\frac{\sum_{i=1}^{i=n}(M_i-O_i)^2}{n}} \quad (17)$$

where M is satellite SM and n is the sample size. Similarly, root mean square deviation (RMSD) and r are also employed to assess the differences between SPL2SMAP (S) and the downscaled SM (D) retrievals in this paper as

$$RMSD = \sqrt{\frac{\sum_{i=1}^{i=n}(S_i-D_i)^2}{n}} \quad (18)$$

$$r_{S,D} = \frac{\sum_{i=1}^{i=n}(S_i-\bar{S})(D_i-\bar{D})}{\sqrt{\sum_{i=1}^{i=n}(S_i-\bar{S})^2\sum_{i=1}^{i=n}(D_i-D)^2}} \quad (19)$$

4 | VALIDATION OF DOWNSCALING METHODS

Comprehensive assessments on advantages and disadvantages of the above approaches were conducted based on agreement statistics with the quality controlled SCAN SM measurements. With respect to the SCAN observations, Figure 1 shows correlations coefficients (r) for 25 km SMAPV5 and l km UCLA_DTR SM data during the May 3, 2017 to April 30, 2019 period. Overall, the UCLA_DTR 1 km SM presents a similar pattern with the original 25 km SMAP. Both SMAPV5 and UCLA_DTR present a good agreement with in situ observations on the CONUS domain except for few scattered stations in the Great Plaints and northeastern area. With respect to the quality controlled in situ SM measurements, the SMAPV5 exhibited stronger correlations (r > 0.70) at 41.5% SCAN sites, which increased slightly to 42.6% by the UCLA_DTR.

Figure 2 shows differences in correlation coefficients between the SMAPV5 and 1 km SMAP SM estimations over the May 3, 2017–April 30, 2019 period. Sites in blue colours indicate that the downscaled 1 km SMAP SM had a stronger agreement with SCAN measurements, whereas in red colours mean that the SMAPV5 performed better. Overall, both TRIA and VTCI methods presented modest performance in comparison with the SMAPV5, while the situation was

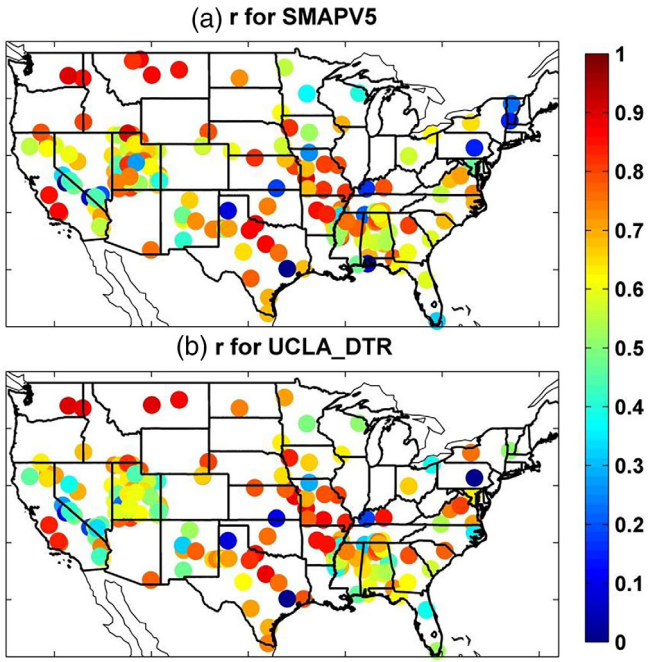

FIGURE 1 Correlations coefficients (r) of the quality controlled SCAN observations for (a) 25 km SMAP and (b) l km UCLA_DTR SM during the May 3, 2017 to April 30, 2019 period

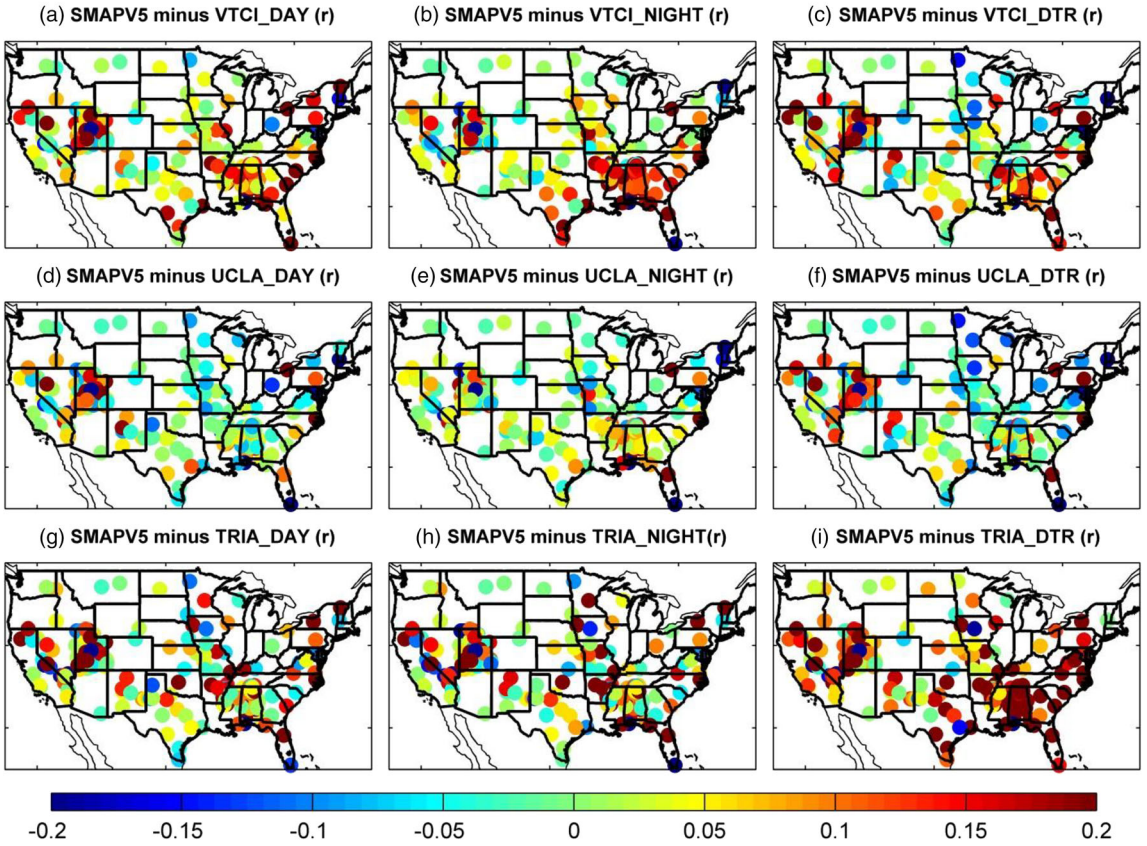

FIGURE 2 Differences in correlation coefficients (*r*) between the original 25 km SMAP5 and the various downscaled 1 km SMAP soil moisture estimations when evaluated against the quality controlled SCAN soil moisture during the May 3, 2017 to April 30, 2019 period. Sites in blue (red) colour indicate the downscaled 1 km SMAP has stronger (weaker) consistency with the SCAN measurements

markedly improved by the UCLA approach. Over the UCLA_DAY and UCLA_NIGHT cases, the UCLA_DTR was more successful in respecting the dynamic trends of the SCAN measurements. Specifically, relative to the SMAPV5 (r = 0.642), the CONUS domain-averaged correlation coefficients were reduced by 0.06 (9.4% reduction versus SMAPV5), 0.058 (9.0% reduction) and 0.046 (7.2% reduction) by the VTCI_DAY, VTCI_NIGHT and VICI_DTR, respectively (Table 1). Similarly, the TRIA method showed a humble behaviour with the CONUS domain-averaged correlation coefficients spanning from 0.576 to 0.582. With benefits of day-time, night-time and diurnal VIIRS LST information, the CONUS domain-averaged correlation coefficients for the corresponding UCLA downscaling schemes were 0.640, 0.632 and 0.642, respectively. The UCLA_DTR showed the strongest consistency with the SCAN observations in the nine downscaling schemes, being also the only one that is comparable to the 25 km SMAPV5.

The original 25 km SMAP SM data product presented reasonable uncertainties (RMSE ≤ 0.1m^3/m^3) in the mid-western CONUS, while having a modest performance in the eastern area which is covered by dense vegetation (Figure 3a).UCLA_DTR showed a relatively better performance with respect to the quality controlled in situ observations (Figure 3b). Compared to SMAPV5, the 1 km SM on basis of UCLA_DTR downscaling strategy exhibited lower RMSEs, not only in

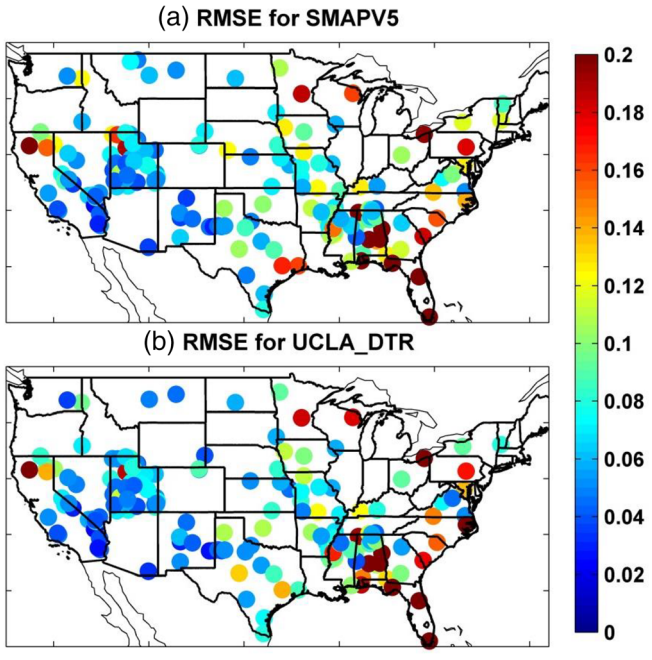

FIGURE 3 RMSE (m^3/m^3) of the quality controlled SCAN observations for (a) 25 km SMAP and (b) l km UCLA_DTR SM during the May 3, 2017 to April 30, 2019 period

the sparsely vegetated west areas but also in the densely vegetated Mississippi river region (Figure 4f). Statistical results demonstrate that the original 25 km SMAP SM had a performance of RMSE ≤ 0.05 m^3/m^3 at 22.3% of SCAN sites, while the UCLA_DTR archived this at 28.4% of sites (6.1% increase versus SMAPV5). Meanwhile, the SMAPV5 SM showed reasonable performance (RMSE ≤ 0.1 m^3/m^3) at 74.3% SCAN sites, which can be increased to 79.1% (4.8% increase versus SMAPV5) by the UCLA_DTR 1 km SM.

With respect to the quality controlled SCAN SM observations, Figure 4 exhibits differences in RMSE between the original SMAPV5 and the downscaled 1 km SMAP soil moisture estimations from May 3, 2017 to April 30, 2019 period. Relative to the original SMAP, the TRIA-based 1 km SMAP exhibited larger errors in the eastern CONUS and the western mountain areas (Figure 4). The VTCI-based 1 km SM was found to be comparable to SMAPV5 in the mid-west CONUS, but presented a modest performance in the densely vegetated areas (Figure 4). However, compared to SMAPV5, the uncertainties were clearly reduced by the UCLA downscaling schemes not only in the western mountain areas but also in the densely vegetated eastern CONUS. Specifically, compared to SMAPV5 (0.089 m^3/m^3), the CONUS domain-averaged RMSEs were increased by 0.008 m^3/m^3 (9.0% increase versus SMAPV5), 0.008 m^3/m^3 (9.0% increase) and 0.002 m^3/m^3 (2.3% increase) by VTCI_DAY, VTCI_NIGHT and VICI_DTR, respectively (Table 2). Similarly, over the 25 km SMAPV5,

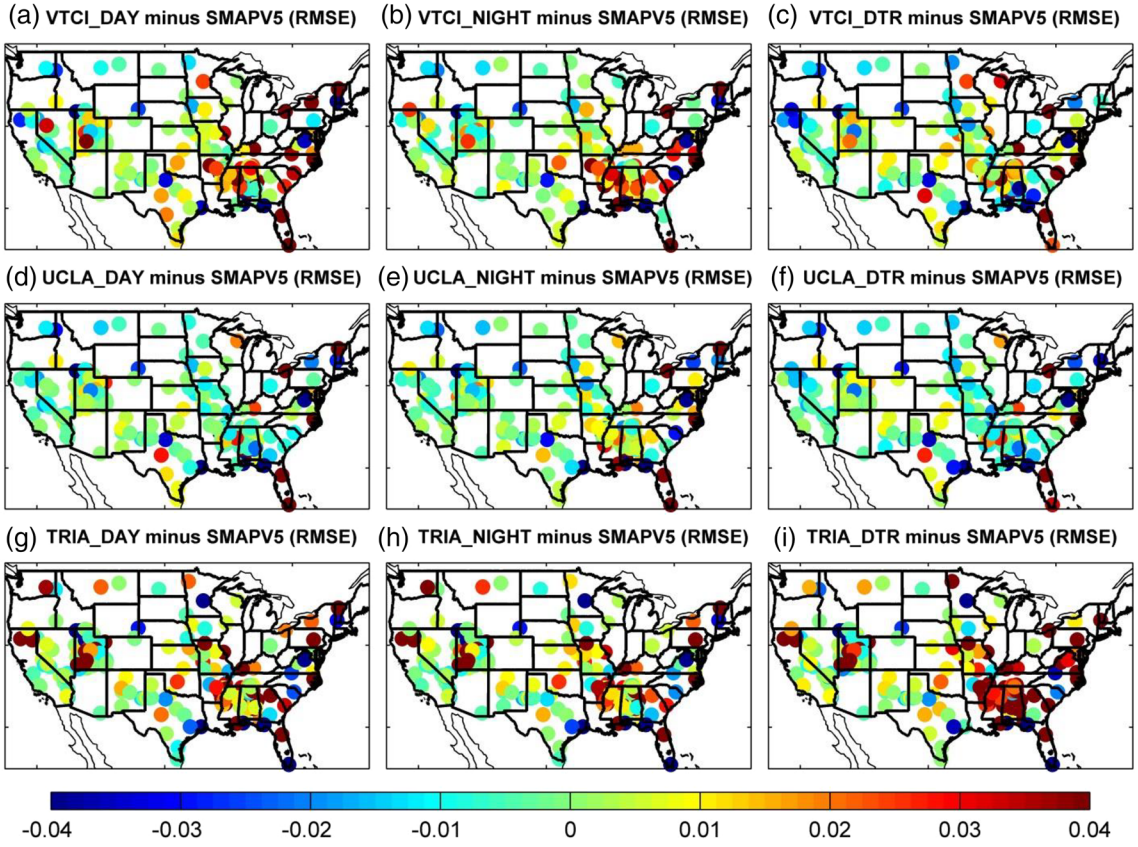

FIGURE 4 Differences in RMSE (m^3/m^3) between the original 25 km SMAP5 and the various downscaled 1 km SMAP soil moisture estimations when evaluated against the quality controlled SCAN soil moisture during the May 3, 2017 to April 30, 2019 period. Sites in blue (red) colour indicate the downscaled 1 km SMAP has stronger (weaker) consistency with the SCAN measurements

TABLE 2 Summary of the statistical comparison results when averaged across the CONUS, including correlation coefficient (*r*), RMSE (m^3/m^3), and ubRMSE (m^3/m^3)

		VTCI			UCLA			TRIA		
Metrics	SMAPV5	DAY	NIGHT	DTR	DAY	NIGHT	DTR	DAY	NIGHT	DTR
R	***0.642***	0.582	0.584	0.596	0.640	0.632	***0.642***	0.576	0.574	0.582
RMSE	0.089	0.091	0.092	0.086	0.084	0.086	***0.082***	0.097	0.097	0.091
ubRMSE	0.054	0.060	0.059	0.054	0.051	0.053	***0.049***	0.062	0.063	0.060

Note: Italic bold indicates the optimal metric, while the abbreviations DAY, NIGHT and DTR means fusion schemes using day-time LST, night-time LST and day-night LST difference, respectively.

the CONUS domain-averaged errors were increased by 0.002 m^3/m^3 (2.3% increase versus SMAPV5) and 0.003 m^3/m^3 (3.4% increase) by VTCI_DAY and VTCI_NIGHT, respectively, while reduced by 0.003 m^3/m^3 (3.4% reduction) by VTCI_DTR. Relative to the 25 km SMAP, the UCLA method showed a better performance with the CONUS domain-averaged RMSEs reduced by 0.05 m^3/m^3 (5.6% reduction versus SMAPV5), 0.03 m^3/m^3 (3.4% reduction) and 0.07 m^3/m^3 (7.9% reduction) by UCLA_DAY, UCLA_NIGHT and UCLA_DTR, respectively.

After the radar stopped operation, the SMAP SM data product had been continuously generated with the radiometer (Yin et al., 2018). The SMAP is expected to archive accurate SM with the expected performance that ubRMSE is less than 0.04 m^3/m^3 (Chan et al., 2016; Colliander et al., 2017). With respect to the quality controlled SCAN measurements, the original 25 km SMAP SM meets the requirement well in the mid-western and southeastern CONUS, whereas larger ubRMSEs can be found in the Mississippi river and northeastern areas (Figure 5a). Relatively, the UCLA_DTR shows a consistently successful behaviour on the CONUS domain (Figure 5b). Specifically, statistical results document that SMAPV5 showed a performance of ubRMSE≤0.04 m^3/m^3at 21.6% of SCAN sites, which increased to 31.8% (10.2% increase versus SMAPV5) by the UCLA_DTR. Validation results also show that SMAPV5 exhibited a good performance (ubRMSE less than 0.05 m^3/m^3) at 49.3% SCAN sites, while the UCLA_DTR performs reasonably at 61.8% (12.5% increase versus SMAPV5) of SCAN sites.

Statistical results document that the CONUS domain-averaged ubRMSE for SMAPV5 was 0.054 m^3/m^3, which increased by 0.006 m^3/m^3 (11.1% increase versus SMAPV5), 0.005 m^3/m^3 (9.3% increase), 0.008 m^3/m^3 (14.8% increase), 0.009 m^3/m^3 (16.7% increase) and 0.006 m^3/m^3 (11.1% increase) by VTCI_DAY, VTCI_NIGHT, TRIA_DAY, TRIA_NIGHT and TRIA_DTR, respectively (Figure 6). However, compared to the 25 km SMAP, UCLA_DAY, UCLA_NIGHT and UCLA_DTR exhibited better performance with reduced ubRMSEs by 0.003 m^3/m^3 (5.7% reduction), 0.001 m^3/m^3 (1.9% reduction) and 0.004 m^3/m^3 (7.4% reduction), respectively (Table 2).

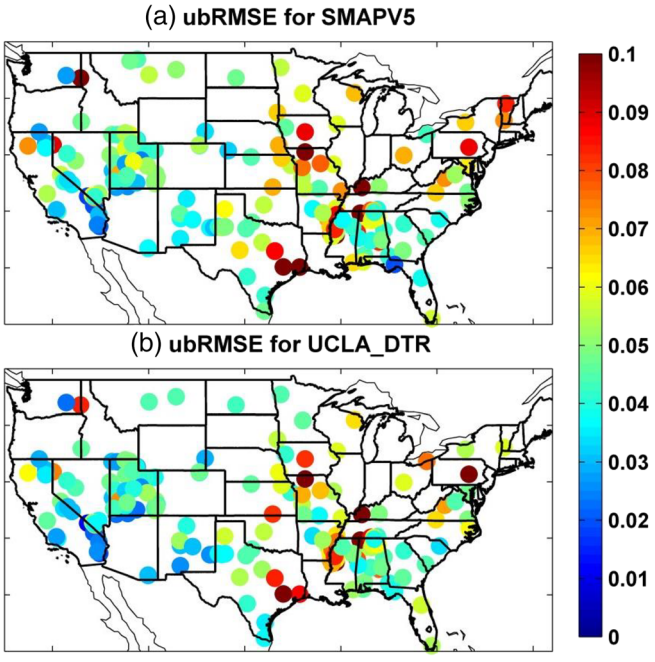

FIGURE 5 UbRMSE (m^3/m^3) of the quality controlled SCAN observations for (a) 25 km SMAP and (b) l km UCLA_DTR SM during the May 3, 2017 to April 30, 2019 period

5 | COMPLEMENTARY EVALUATIONS WITH COMPARING WITH SPL2SMAP

The downscaled 1 km SMAP SM based on the UCLA_DTR method was upscaled to 3 km spatial resolution (UCLA_DTRup) to match the grid of the 3 km SPL2SMAP SM data product. Figure 7 shows the UCLA_DTRup versus the SPL2SMAP SM over the CONUS domain from May 1, 2017 to April 30, 2019. The correlation coefficient *r* value is 0.834, which implies that variation trends between UCLA_DTRup and SPL2SMAP SM match well. However, the large RMSD value (0.071 m^3/m^3) indicates that their differences are remarkable. In particular, it can be found that the UCLA_DTRup and SPL2SMAP match well in dry (SM less than 0.2 m^3/m^3) areas. However, wetter patterns of SPL2SMAP in the wet areas led to the lower sample density area with shading in the blue colour departing from the ideal regression curve. The situation was significantly improved when the 3 km SPL2SMAP was quality controlled by excluding the measurements outside of the physically possible range (SM greater than 0.50 m^3/m^3). After quality control, the UCLA_DTRup showed a robust agreement with the SPL2SMAP with the regression curve shifting towards the perfectly matched line. Benefits of the quality control are also seen by improvements in *r* value from 0.834 to 0.845, and the RMSD from 0.071 to 0.057 m^3/m^3.

Based on the quality controlled SCAN measurements, validations on SPL2SMAP and UCLA_DTRup 3 km SM estimations were conducted on the CONUS domain (Figure 8). The SPL2SMAP is well consistent with the SCAN observations in the middle-southern and north-western CONUS, while having a modest performance in the western-mountain and central-eastern areas (Figure 8a). However, the UCLA_DTRup presents a much stronger agreement with in situ observations over the entire CONUS domain except in the middle-southern region. Specifically, statistical results indicate that SPL2SMAP had $r > 0.5$ at 67.8% SCAN sites, while UCLA_DTRup had reasonable behaviour $r > 0.5$ at 78.5% stations (10.7% increase versus SPL2SMAP). The CONUS domain-averaged correlation coefficient for the SPL2SMAP was 0.532, which increased to 0.620 (16.5% increase versus SPL2SMAP) by the UCLA_DTRup (Figure 8b).

Regarding the uncertainties, SPL2SMAP showed a strong gradient of lower RMSEs in the west to higher errors in the east (Figure 8c). Compared to the SPL2SMAP, the UCLA_DTRup typically exhibited a better performance in densely vegetated areas and a comparable behaviour in sparsely vegetated regions. Specifically, UCLA_DTRup

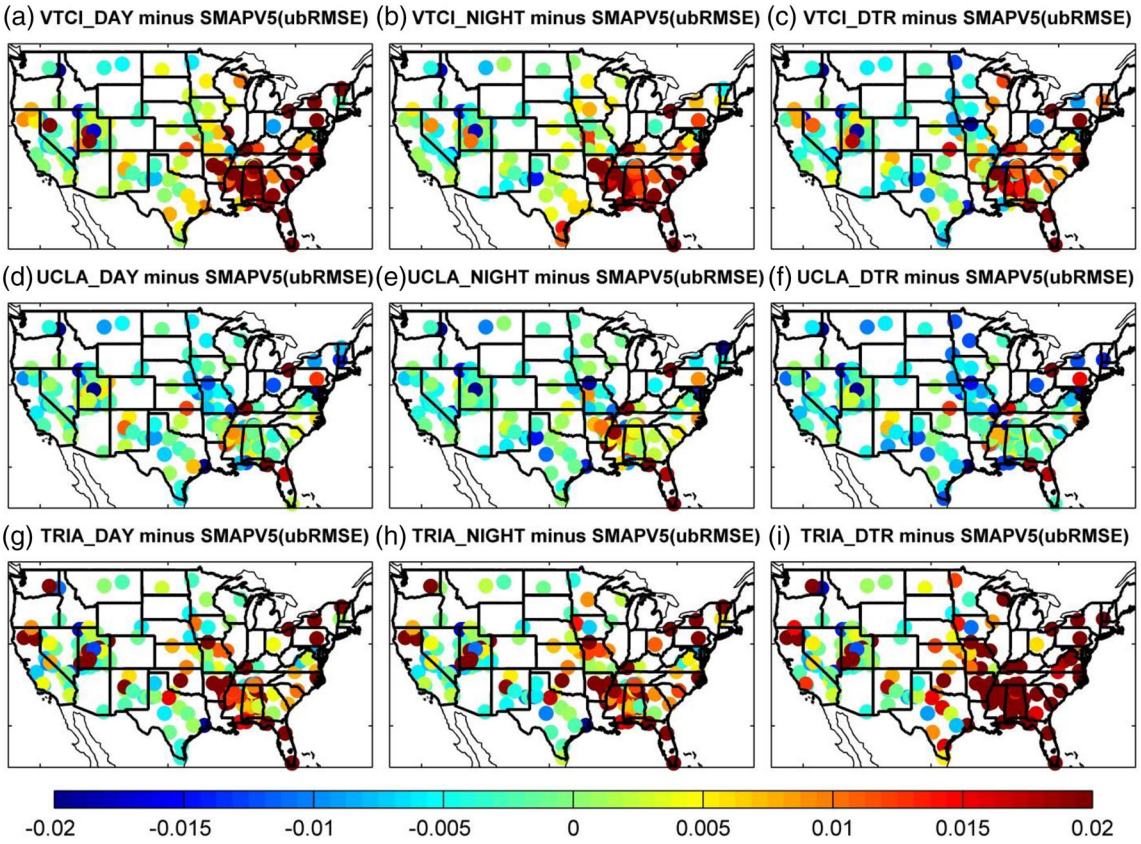

FIGURE 6 Differences in ubRMSE (m^3/m^3) between the original 25 km SMAP5 and the various downscaled 1 km SMAP soil moisture estimations when evaluated against the quality controlled SCAN soil moisture during the May 3, 2017 to April 30, 2019 period. Sites in blue (red) colour indicate the downscaled 1 km SMAP has stronger (weaker) consistency with the SCAN measurements

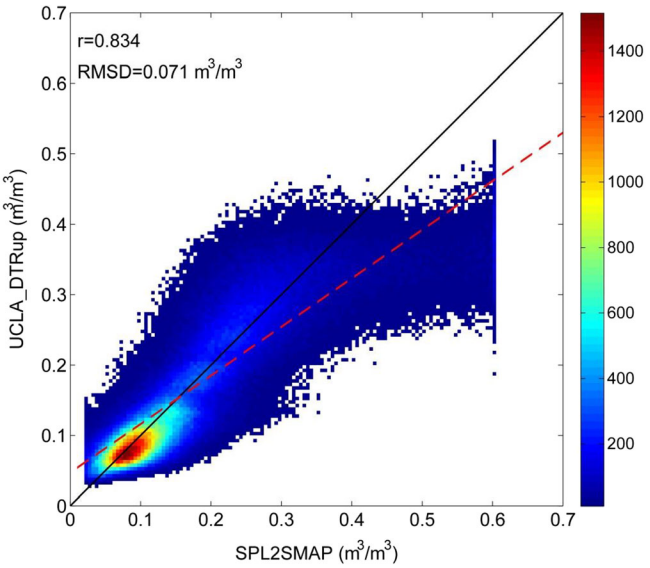

FIGURE 7 The UCLA_DTRup versus the SPL2SMAP from May 1, 2017 to April 30, 2019

showed reasonable uncertainties (RMSE ≤ 0.1 m^3/m^3) at 75.2% of SCAN sites, yet it is declined to 65.3% by the SPL2SMAP. The CONUS domain-averaged RMSE for the NASA 3 km SMAP was 0.0975 m^3/m^3, which was reduced by 0.014 m^3/m^3 (14.4% reduction versus SPL2SMAP) by the UCLA_DTRup (Figure 8d).

Additionally, the SPL2SMAP showed lower ubRMSEs in the western and south-eastern CONUS, whereas a modest performance was found in the Mississippi River and the north-eastern areas (Figure 8e). Particularly, the 3 km SMAP met the target of the SMAP mission (ubRMSE less than 0.04 m^3/m^3) at 17.4% SCAN sites, while dramatically increasing to 34.7% (17.3% increase versus SPL2SMAP) by the UCLA_DTRup. Besides, the SPL2SMAP documented a reasonable performance (ubRMSE less than 0.05 m^3/m^3) at 38.8% stations, raising to 62.8% (24.0% increase versus SPL2SMAP) by the UCLA_DTRup (Figure 8e). The CONUS domain-averaged ubRMSEs for SPL2SMAP and UCLA_DTRup were 0.065 and 0.049 m^3/m^3 (32.7% reduction versus SPL2SMAP), respectively.

With respect to the quality controlled SCAN SM measurements, validation metrics including correlation coefficients, RMSE and ubRMSE showed that the UCLA_DTRup had an overwhelming advantage over the 3 km NASA SPL2SMAP SM product, with significantly decreased uncertainties and raised the agreement with in situ observations. To inter-compare SPL2SMAP and the downscaled SM estimations in a fair way, the UCLA_DTR was upscaled to 3 km spatial resolution, but it cannot overshadow the better performance of the downscaled 1 km SM. Given UCLA_DTR 1 km SM presents a much

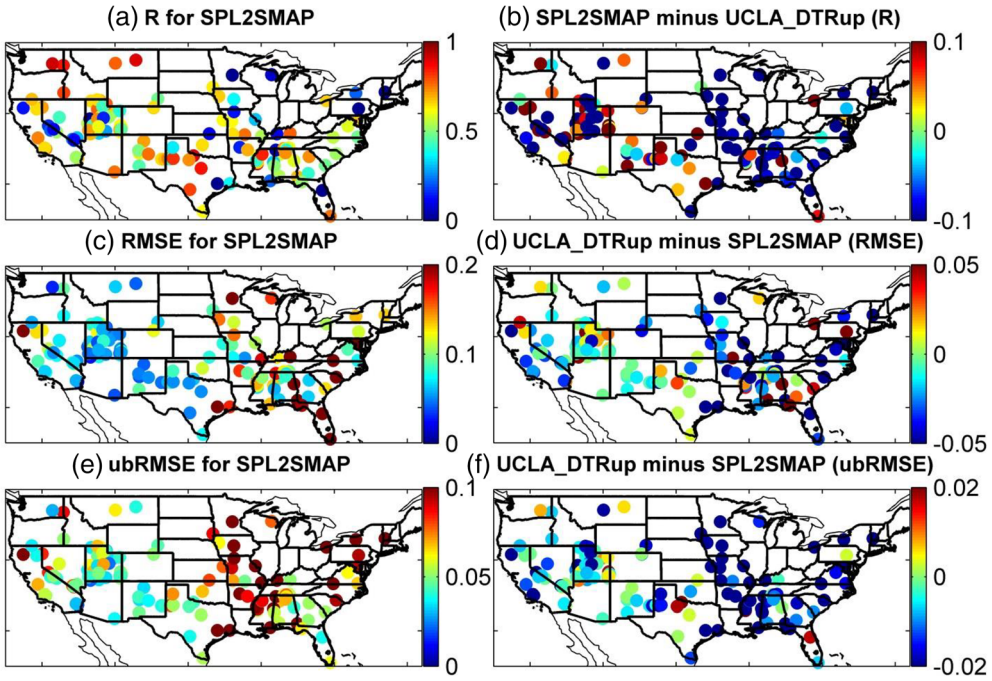

FIGURE 8 With respect to the quality controlled SCAN soil moisture observations, left column shows the metrics for SPL2SMAP, while the right column shows metric differences between SPL2SMAP and UCLA_DTRup during the May 1, 2017–April 30, 2019 period. Top, middle and bottom rows are for correlation coefficients (*r*), RMSE and ubRMSE, respectively

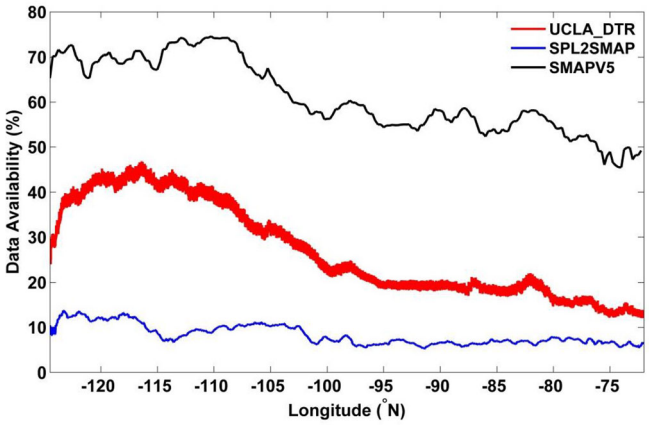

FIGURE 9 Longitude-averaged data availability (Unit: %) for 25 km SMAPV5, 3 km SPL2SMAP and 1 km UCLA_DTR soil moisture estimations over the CONUS domain over the May 1, 2017–April 30, 2019 period

better behaviour (Table 2) in comparison with UCLA_DTRup, the statistical results can certainly mirror the developed 1 km SMAP data product on the basis that the UCLA_DTR method may achieve accurate fine spatial resolution SM.

Data availability is defined as the fraction of available day number for each land grid over total day number during the study period (Yin, Zhan, et al., 2019). On the CONUS domain, the longitude-averaged data availability (LDA) for the original 25 km SMAP presented a strong west–east gradient with 70% longitude-averaged data availability (LDA) in the western regions and 50% LDA in the densely vegetated eastern area (Figure 9). Based on fine resolution C-band Sentinel-1 backscatters, SMAP Tb was downscaled to generated the 3 km SMAP SM data. Revisit time for Sentinel-1 is 12-day, but the combination of Sentinel-1A and -1B offers a 6-day repeat cycle. The low revisit rate of Sentinel-1 leads to small LDA spanning from 10% to 15% for the SPL2SMAP SM product (Figure 9). Compared to the NASA 3 km SMAP, the LDA can be significantly improved by the downscaled 1 km SM data. In the eastern CONUS, LDA for the 1 km SMAP was around 20%, while reaching to 45% in the western CONUS. The low LDA for the UCLA_DTR 1 km in the eastern areas is not only resulted from the strong west–east LDA gradient of the original coarse resolution SMAP, but also affected by the larger cloud cover in the eastern wetter areas.

6 | OPERATIONAL PATHWAY

Building on the satellite LST and EVI measurements, the UCLA_DTR-based 1 km SMAP SM had the best performance out of the 9 downscaling schemes tested with respect to the quality controlled SCAN observations. The strong station-to-station and year-to-year consistency of the results shown in Sections 4 and 5 document that the validations are qualitatively stable and should be representative of a longer analysis period, permitting operational production of the NRT 1 km SMAP SM at NOAA-STAR using the UCLA_DTR method. Since the LST and VI products are available daily only, the 1 km SM product can only be generated daily with a latency limited by the SMAP TB. The NASA official SMAPV5 SM product used for this study allowed the 1 km and the NASA 3 km SPL2SMAP SM data to be inter-compared in a fair way. NOAA-STAR has developed the NRT 25 km SMAP SM with about 2-hour latency, which is much shorter than the official SMAP data product at NASA (Zhan et al., 2016).

The 1 km SMAP SM algorithm consists of the following major functions as Figure 10: (a) a pre-processing function is designed to

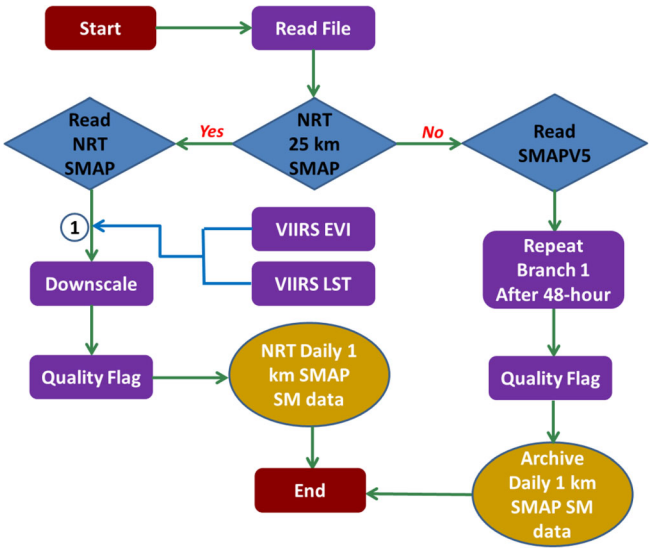

FIGURE 10 Process flow of producing a NRT 1 km downscaled SMAP soil moisture map using the UCLA_DTR method

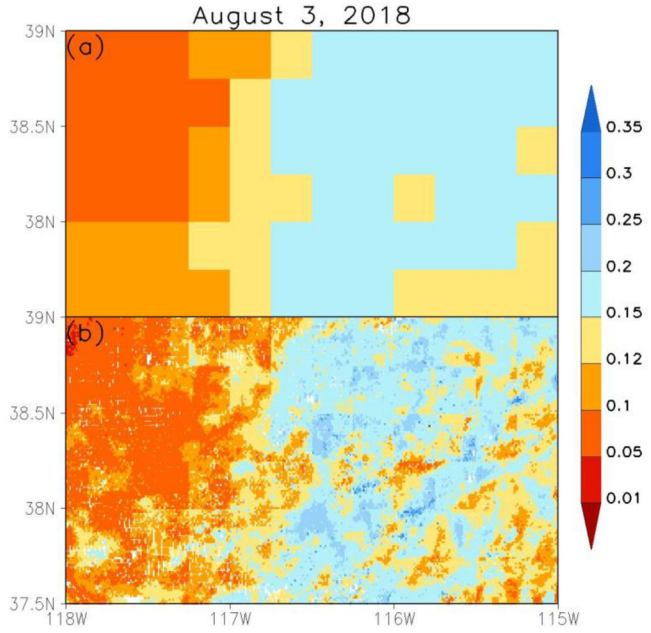

FIGURE 11 Sample maps for (a) SMAPV5 25 km and (b) the downloaded 1 km SMAP SM retrievals over the sub-region from −118°E, 37.5°N to 115°E, 39°N on August 3, 2018

ingest the required input data including 1 km VIIRS LST and EVI retrievals, as well as the SMAP SM data. The process is stopped if any validity or quality assessment is invalid. (b) The NRT branch runs when the NOAA-STAR NRT SMAP is available. The NRT daily 1 km SMAP SM data will be produced using the UCLA_DTR downscaling strategy if the current processing time is the end of the day. Based on quality assessments of the input data, quality flag bits are generated grid-by-grid with "0" indicating bad and "1" representing good. (c) Daily metadata and quality flag layers are produced and the corresponding status report file generated, and then the NRT daily 1 km SMAP SM product is delivered to operational users. (d) The NASA official SMAPV5 is expected to have the highest quality compared to other coarse resolution radiometer SM retrievals. Thus, an archive run is activated to produce a daily 1 km SMAP SM product for archiving after 48-hour using the SMAPV5. Similarly, quality flag bits are also generated grid-by-grid with "0" indicating bad and "1" representing good. The daily archived 1 km SMAP SM product is then delivered to operational users.

Figure 11 shows sample maps for SMAPV5 25 km and the downloaded 1 km SMAP SM retrievals over the sub-region from −118°E, 37.5°N to 115°E, 39°N on August 3, 2018. The 1 and 25 km SMAP SM maps display quite similar wet and dry patterns over the sub-region domain. The original 25 km SMAP SM shows a strong west-to-east gradient over the sub-region, which can be well captured by the downscaled 1 km SM. As expected, the UCLA_DTR 1 km SM presents much more spatial detail, which may highlight the advantages of the 1 km SMAP SM.

7 | CONCLUSIONS

Based on satellite LST and EVI observations, a fine scale SMAP soil moisture data product was developed to meet the requirements of regional meteorological, hydrological and agricultural applications. The advantages of the downscaling technique include simplicity, feasibility of operational implementation, pure reliance on remote sensing measurements, computationally fast and limited ancillary information requirements. With respect to the quality controlled SCAN observations, the UCLA_DTR method showed the most successful performance out of the nine downscaling schemes, raising correlation coefficients and decreasing uncertainties. Compared to the original coarse spatial resolution SMAP, the downscaled 1 km SM data product presents much more spatial details. As expected, the accuracy level is significantly improved with the advance of the fine scale satellite SM measurements.

Compared to the NASA 3 km SMAP/Sentinel product, the accuracy level was significantly improved. The downscaled 1 km SMAP SM data product also provides larger data availability, although the VIIRS observations used as ancillary information can be affected by cloud coverage. Building on the results shown in this paper, a near real time 1 km SMAP SM data product is proposed to be developed at NOAA-NESDIS (National Environmental Satellite, Data, and Information Service)-STAR.

ACKNOWLEDGEMENTS

This work was jointly supported by National Oceanic and Atmospheric Administration's Climate Program Office's Modelling, Analysis, Predictions, NASA SMAP Science Utilization Program and NOAA JPSS Proving Ground and Risk Reduction (PGRR) Program. We would like to thank Dr Yuling Liu and Dr Yunyue Yu from NOAA-NESDIS-SATR for providing the VIIRS land surface temperature measurements. The manuscript contents are solely the opinions of the authors and do not constitute a statement of policy, decision, or position on behalf of NOAA or the US Government.

DATA AVAILABILITY STATEMENT

The NASA 3 km SMAP/Sentinel soil moisture observations that support the findings of this study are openly available in https://nsidc.org/data/spl2smap_s. The 25 km SMAP soil moisture data can be obtained from NOAA-NESDIS Office of Satellite and Product Operations at http://www.ospo.noaa.gov/Products/land/smops/smops_loops.html.

ORCID

Jifu Yin https://orcid.org/0000-0002-7782-6519

REFERENCES

Abbaszadeh, P., Moradkhani, H., & Zhan, X. (2019). Downscaling SMAP radiometer soil moisture over the CONUS using an ensemble learning method. *Water Resources Research*, *55*, 324–344.

Alemohammad, S. H., Kolassa, J., Prigent, C., Aires, F., & Gentine, P. (2018). Global downscaling of remotely sensed soil moisture using neural networks. *Hydrology and Earth System Sciences*, *22*, 5341–5356.

Carlson, T. N., Gillies, R. R., & Perry, E. M. (1994). A method to make use of thermal infrared temperature and NDVI measurements to infer surface soil water content and fractional vegetation cover. *Remote Sensing Reviews*, *9*(1–2), 161–173.

Chan, S. K., Bindlish, R., O'Neill, P. E., Njoku, E., Jackson, T., Colliander, A., … Kerr, Y. (2016). Assessment of the SMAP passive soil moisture product. *IEEE Transactions on Geoscience and Remote Sensing*, *54*(8), 4994–5007.

Colliander, A., Jackson, T. J., Bindlish, R., Chan, S., Das, N., Kim, S. B., … Yueh, S. (2017). Validation of SMAP surface soil moisture products with core validation sites. *Remote Sensing Reviews*, *191*, 215–231.

Das, N. N., Entekhabi, D., Dunbar, R. S., Chaubell, M. J., Colliander, A., Yueh, S., … Thibeault, M. (2019). The SMAP and Copernicus sentinel 1A/B microwave active-passive high resolution surface soil moisture product. *Remote Sensing Reviews*, *233*, 111380. https://doi.org/10.1016/j.rse.2019.111380

Das, N. N., Entekhabi, D., Kim, S., Yueh, S., & O'Neill, P. (2016). Combining SMAP and sentinel data for high-resolution soil moisture product. *2016 IEEE International Geoscience and Remote Sensing Symposium (IGARSS)*, (129–131). IEEE.

Das, N. N., Entekhabi, D., Njoku, E. G., Shi, J. J. C., Johnson, J. T., & Colliander, A. (2014). Tests of the SMAP combined radar and radiometer algorithm using airborne field campaign observations and simulated data. *IEEE Transactions on Geoscience and Remote Sensing*, *52*(4), 2018–2028.

Dobriyal, P., Qureshi, A., Badola, R., & Hussain, S. A. (2012). A review of the methods available for estimating soil moisture and its implications for water resource management. *Journal of Hydrology*, *458–459*, 110–117.

Entekhabi, D., N. Das, E. Njoku, S. Yueh, J. Johnson, J. Shi. 2014. Algorithm Theoretical Basis Document L2 & L3 Radar/Radiometer Soil Moisture (Active/Passive) Data Products. Revision A, December 2014. JPL, California Institute of Technology.

Entekhabi, D., Njoku, E. G., O'Neill, P. E., Kellogg, K. H., Crow, W. T., Edelstein, W. N., … Van Zyl, J. (2010). The Soil Moisture Active Passive (SMAP) mission. *Proceedings of the IEEE*, *98*(5), 704–716.

Fang, B., Lakshmi, V., Bindlish, R., & Jackson, T. J. (2018). Downscaling of SMAP soil moisture using land surface temperature and vegetation data. *Vadose Zone Journal*, *17*, 170198. https://doi.org/10.2136/vzj2017.11.0198

He, L., Hong, Y., Wu, X., Ye, N., Walker, J. P., & Chen, X. (2018). Investigation of SMAP active–passive downscaling algorithms using combined Sentinel-1 SAR and SMAP radiometer data. *IEEE Transactions on Geoscience and Remote Sensing*, *56*(8), 4906–4917.

Huete, A., Didan, K., Miura, T., Rodriguez, E. P., Gao, X., & Ferreira, L. G. (2002). Overview of the radiometric and biophysical performance of the MODIS vegetation indices. *Remote Sensing of Environment*, *83*(1–2), 195–213.

Jackson, T. J., & O'Neill, P. E. (1990). Attenuation of soil microwave emission by corn and soybeans at 1.4 and 5 GHz. *IEEE Transactions on Geoscience and Remote Sensing*, *28*(5), 978–980.

Jackson, T. J., & Schmugge, T. J. (1989). Passive microwave remote sensing system for soil moisture: Some supporting research. *IEEE Transactions on Geoscience and Remote Sensing*, *27*(2), 225–235.

JAXA. (2013). Descriptions of GCOM-W1 AMSR2 level 1R and level 2 algorithms. NDX-120015A. Jul., *9*, 108–119.

Jiang, L., & Islam, S. (2003). An intercomparison of regional latent heat flux estimation using remote sensing data. *International Journal of Remote Sensing*, *24*(11), 2221–2236.

Kerr, Y. H. (2007). Soil moisture from space: Where are we? *Hydrogeology Journal*, *15*(1), 117–120.

Kerr, Y. H., Waldteufel, P., Wigneron, J.-P., Delwart, S., Cabot, F., Boutin, J., … Mecklenburg, S. (2010). The SMOS mission: New tool for monitoring key elements of the globalwater cycle. *Proceedings of the IEEE*, *98*(5), 666–687.

Kim, J., & Hogue, T. S. (2012). Improving spatial soil moisture representation through integration of AMSR-E and MODIS products. *IEEE Transactions on Geoscience and Remote Sensing*, *50*(2), 446–460.

Knipper, K. R., Hogue, T. S., Franz, K. J., & Scott, R. L. (2017). Downscaling SMAP and SMOS soil moisture with moderate-resolution imaging spectroradiometer visible and infrared products over southern Arizona. *Journal of Applied Remote Sensing*, *11*(2), 026021. https://doi.org/10.1117/1.JRS.11.026021

Li, J., Wang, S., Gunn, G., Joosse, P., & Russell, H. A. J. (2018). A model for downscaling SMOS soil moisture using Sentinel-1 SAR data. *International Journal of Applied Earth Observation*, *72*, 109–121.

Li, L., Gaiser, P. W., Gao, B.-C., Bevilacqua, R. M., Jackson, T. J., Njoku, E. G., … Bindlish, R. (2010). WindSat global soil moisture retrieval and validation. *IEEE Transactions on Geoscience and Remote Sensing*, *48*(5), 2224–2241.

Liu, W., Baret, F., Gu, X., Tong, X., Zheng, L., & Zhang, B. (2002). Relating soil surface moisture to reflectance. *Remote Sensing of Environment*, *81*(2–3), 238–246.

Liu, Q., Reichle, R. H., Bindlish, R., Cosh, M. H., Crow, W. T., & de Jeu, R. (2011). The contributions of precipitation and soil moisture observations to the skill of soil moisture estimates in a land data assimilation system. *Journal of Hydrometeorology*, *12*(5), 750–765.

Liu, Y., Yu, Y., Yu, P., Göttsche, F., & Trigo, I. (2015). Quality assessment of S-NPP VIIRS land surface temperature product. *Remote Sensing*, *7*(9), 12215–12241.

Liu, Y., Yu, Y., Yu, P., Wang, H., & Rao, Y. (2019). Enterprise LST algorithm development and its evaluation with NOAA 20 data. *Remote Sensing*, *11*, 2003. https://doi.org/10.3390/rs11172003

Merlin, O., Chehbouni, A., Kerr, Y. H., & Goodrich, D. C. (2006). A downscaling method for distributing surface soil moisture within a microwave pixel: Application to the monsoon '90 data. *Remote Sensing of Environment*, *101*, 379–389.

Merlin, O., Chehbouni, G., Kerr, Y., Njoku, E. G., & Entekhabi, D. (2005). A combined modeling and multi-spectral/multi-resolution remote sensing approach for disaggregation of surface soil moisture: Application to SMOS configuration. *IEEE Transactions on Geoscience and Remote Sensing*, *43*(9), 2036–2050.

Merlin, O., Walker, J. P., Kalma, J. D., Kim, E. J., Hacker, J., Panciera, R., … Jackson, T. J. (2008). The NAFE'06 data set: Towards soil moisture retrieval at intermediate resolution. *Advances in Water Resources*, *31*, 1444–1455.

Mishra, V., Ellenburg, W. L., Griffin, R. E., Mecikalski, J. R., Cruisea, J. F., Hain, C. R., & Anderson, M. C. (2018). An initial assessment of a SMAP soil moisture disaggregation scheme using TIR surface evaporation

data over the continental United States. *International Journal of Applied Earth Observation*, *68*, 92–104.

Miura, T., Muratsuchi, J., & Vargas, M. (2018). Assessment of cross-sensor vegetation index compatibility between VIIRS and MODIS using near-coincident observations. *Journal of Applied Remote Sensing*, *12*(4), 045004. https://doi.org/10.1117/1.JRS.12.045004

Molero, B., Merlin, O., Malbéteau, Y., Al Bitar, A., Cabot, F., Stefan, V., & Jackson, T. J. (2016). SMOS disaggregated soil moisture product at 1 km resolution: Processor overview and first validation results. *Remote Sensing of Environment*, *180*, 361–376.

Narayan, U., Lakshmi, V., & Jackson, T. H. (2006). High-resolution change estimation of soil moisture using L-band radiometer and radar observations made during the SMEX02 experiments. *IEEE Transactions on Geoscience and Remote Sensing*, *44*, 1545–1554.

Njoku, E. G., Jackson, T. J., Lakshmi, V., Chan, T. K., & Nghiem, S. V. (2003). Soil moisture retrieval from AMSR-E. *IEEE Transactions on Geoscience and Remote Sensing*, *41*(2), 215–229.

Peng, J., Loew, A., Merlin, O., & Verhoest, N. E. C. (2017). A review of spatial downscaling of satellite remotely sensed soil moisture. *Reviews of Geophysics*, *55*, 341–366.

Peng, J., Loew, A., Zhang, S., Wang, J., & Niesel, J. (2016). Spatial downscaling of satellite soil moisture data using a vegetation temperature condition index. *IEEE Transactions on Geoscience and Remote Sensing*, *54*(1), 558–566.

Petropoulos, G. P., Carlson, T. N., Wooster, M. J., & Islam, S. (2009). A review of Ts/VI remote sensing based methods for the retrieval of land surface energy fluxes and soil surface moisture. *Progress in Physical Geography*, *33*(2), 224–250.

Piles, M., Camps, A., Vall-llossera, M., Corbella, I., Panciera, R., Rüdiger, C., … Kerr, Y. H. (2011). Downscaling SMOS-derived soil moisture using MODIS visible/infrared data. *IEEE Transactions on Geoscience and Remote Sensing*, *49*(9), 3156–3166.

Reichle, R. H., De Lannoy, G. J., Liu, Q., Ardizzone, J. V., Colliander, A., Conaty, A., … Zeng, Y. (2017). Assessment of the SMAP level-4 surface and root-zone soil moisture product using in situ easurements. *Journal of Hydrometeorology*, *18*(10), 2621–2645.

Robinson, D. A., Campbell, C. S., Hopmans, J. W., Hornbuckle, B. K., Jones, S. B., Knight, R., … Wendroth, O. (2008). Soil moisture measurement for ecological and hydrological watershed-scale observatories: A review. *Vadose Zone J.*, *7*(1), 358–389. 10.2136/vzj2007.0143.

Sabaghy, S., Walker, J. P., Renzillo, L. J., & Jackson, T. J. (2018). Spatially enhanced passive microwave derived soil moisture: Capabilities and opportunities. *Remote Sensing of Environment*, *209*, 551–580.

Sandholt, I., Rasmussen, K., & Andersen, J. (2002). A simple interpretation of the surface temperature/vegetation index space for assessment of surface moisture status. *Remote Sensing Environment*, *79* (2/3), 213–224.

Schaefer, G. L., Cosh, M. H., & Jackson, T. J. (2007). The USDA Natural Resources Conservation Service Soil Climate Analysis Network (SCAN). *Journal of Atmospheric and Oceanic Technology*, *24*(12), 2073–2077.

Senanayake, I. P., Yeo, I.-Y., Tangdamrongsub, N., Willgoose, G. R., Hancock, G. R., Wells, T., … Walker, J. P. (2019). An in-situ data based model to downscale radiometric satellite soil moisture products in the upper hunter region of NSW, Australia. *Journal of Hydrology*, *572*, 820–838.

Vereecken, H., Huisman, J. A., Pachepsky, Y., Montzka, C., van der Kruk, J., Bogena, H., … Vanderborght, J. (2014). On the spatio-temporal dynamics of soil moisture at the field scale. *Journal of Hydrology*, *516*, 76–96.

Wagner, W., Hahn, S., Kidd, R., Melzer, T., Bartalis, Z., & Hasenauer, S., … Rubel, F. (2013). The ASCAT soil moisture product: A review of its specifications, validation results, and merging applications. *Meteorologische Zeitschrift*, *22*, 5–33.

Wan, Z., Wang, P., & Li, X. (2004). Using MODIS land surface temperature and normalized difference vegetation index products for monitoring drought in the southern Great Plains, USA. *International Journal of Remote Sensing*, *25*(1), 61–72.

Wang, J. R., ET Engman, T., Mo, T. J., & Schmugge, J. C. S. (1987). The effects of soil moisture, surface roughness, and vegetation on L-band emissions and backscatter. *IEEE Transactions on Geoscience and Remote Sensing*, *GE-25*(6), 825–833.

Wu, X., Walker, J. P., Rüdiger, C., Panciera, R., & Gao, Y. (2017). Intercomparison of alternate soil moisture downscaling algorithms using active–passive microwave observations. *IEEE Transactions on Geoscience and Remote Sensing Letters*, *14*(2), 179–183.

Yin, J., Hain, C. R., Zhan, X., Dong, J., & Ek, M. (2019). Improvements in the forecasts of near surface variables in the global forecast system (GFS) via assimilating ASCAT soil moisture retrievals. *Journal of Hydrology*, *578*, 124018. https://doi.org/10.1016/j.jhydrol.2019.124018

Yin, J., & Zhan, X. (2018). Impact of bias-correction methods on effectiveness of assimilating SMAP soil moisture data into NCEP global forecast system using the ensemble Kalman filter. *IEEE Geoscience and Remote Sensing Letters*, *15*(5), 659–663.

Yin, J., Zhan, X., Hain, C. R., Liu, J., & Anderson, M. C. (2018). A method for objectively integrating soil moisture satellite observations and model simulations toward a blended drought index. *Water Resources Research*, *54*(9), 6772–6791.

Yin, J., Zhan, X., Liu, J., & Schull, M. (2019). An intercomparison of Noah model skills with benefits of assimilating SMOPS blended and individual soil moisture retrievals. *Water Resources Research*, *55*, 2572–2592.

Yin, J., Zhan, X., Zheng, Y., Hain, C. R., Ek, M., Wen, J., … Liu, J. (2016). Improving Noah land surface model performance using near real time surface albedo and green vegetation fraction. *Agricultural and Forest Meteorology*, *218-219*, 171–183.

Yin, J., Zhan, X., Zheng, Y., Liu, J., Fang, L., & Hain, C. R. (2015). Enhancing model skill by assimilating SMOPS blended soil moisture product into Noah land surface model. *Journal of Hydrometeorology*, *16*(2), 917–931.

Yin, J., Zhan, X., Zheng, Y., Liu, J., Hain, C. R., & Fang, L. (2014). Impact of quality control of satellite soil moisture data on their assimilation into land surface model. *Geophysical Research Letters*, *41*, 7159–7166.

Yin, J., Zheng, Y., Zhan, X., Hain, C. R., Zhai, Q., Duan, C., … Fang, L. (2015). An assessment of impacts of land-cover changes on root-zone soil moisture. *International Journal of Remote Sensing*, *36*(24), 6116–6134.

Zhan, X., Houser, P. R., Walker, J. P., & Crow, W. T. (2006). A method for retrieving high-resolution surface soil moisture from Hydros L-band radiometer and radar. *IEEE Transactions on Geoscience and Remote Sensing*, *44*(6), 1534–1544.

Zhan, X., Liu, J., Wen, J., Zhao, L., Vargas, M., & Weng, F. (2016). Soil moisture data product Generated from NASA SMAP observations with NOAA ancillary data. *IEEE International Geoscience and Remote Sensing Symposium*, July 10–15, 5237–5240. https://doi.org/10.1109/IGARSS.2016.7730364

Zhao, W., N Sánchez, H. L., & Li, A. (2018). A spatial downscaling approach for the SMAP passive surface soil moisture product using random forest regression. *Journal of Hydrology*, *563*, 1009–1024.

How to cite this article: Yin J, Zhan X, Liu J, Moradkhani H, Fang L, Walker JP. Near-real-time one-kilometre Soil Moisture Active Passive soil moisture data product. *Hydrological Processes*. 2020;1–14. https://doi.org/10.1002/hyp.13857